coatings

MDPI

Article

Improvement of Optical Confinement for Terahertz Vertical-Cavity Surface-Emitting Laser with Square-Lattice Photonic Crystal Structure

Yadi Wang [1,2], Masanobu Haraguchi [2], Xingbo Zhang [1], Pingping Wang [1,3] and Shufeng Sun [1,*]

[1] Collaborative Innovation Center for Green Intelligent Laser Manufacturing Technology and Equipment of Shandong Province, School of Mechanical and Automotive Engineering, Qingdao University of Technology, Qingdao 266520, China
[2] Institute of Post-LED Photonics, Tokushima University, Tokushima 770-8506, Japan
[3] Collage of Intelligent Manufacturing, Qingdao Huanghai University, Qingdao 266427, China
* Correspondence: sunshufeng@qut.edu.cn

Abstract: A new method proposed to enhance the optical confinement of the terahertz band in a vertical cavity surface emitting laser involves introducing a square-lattice photonic crystal structure. This structure's filling factor was optimized by computing the energy band structure and optical band values of the photonic crystal. The optimal optical band value is 0.436–0.528 a/λ. At a specific carrier concentration, the real part of dielectric constant of GaAs/AlGaAs materials will gradually increase with the increase of Al elements. By adjusting the length of the resonant cavity, a vertical cavity surface emitting laser with two wavelengths can be created without utilizing current injection. Additionally, the photonic crystal structure's control effect on the transverse mode of the vertical cavity surface emitting laser and the release effect of the PN junction light confinement were analyzed. Numerical calculations indicated that incorporating a cubic photonic crystal structure in the vertical cavity surface emitting laser resulted in a 2× increase in the difference frequency intensity and a 6.33× increase in the optical field intensity.

Keywords: vertical cavity surface emitting laser; square-lattice photonic crystal structure; dielectric constant; terahertz wave; optical field intensity

Citation: Wang, Y.; Haraguchi, M.; Zhang, X.; Wang, P.; Sun, S. Improvement of Optical Confinement for Terahertz Vertical-Cavity Surface-Emitting Laser with Square-Lattice Photonic Crystal Structure. *Coatings* **2023**, *13*, 972. https://doi.org/10.3390/coatings13060972

Academic Editor: Alicia de Andrés

Received: 3 April 2023
Revised: 17 May 2023
Accepted: 18 May 2023
Published: 23 May 2023

1. Introduction

In recent years, terahertz wave, with a wavelength in the range of 0.03–3 mm between microwave and far-infrared wave and a frequency of as high as 0.1–10 THz, has been widely studied as a core technology for terahertz optical imaging, ultra-high-speed wireless communication, next-generation homes, and other applications [1,2]. With its advantages of low energy consumption, strong penetration, wide bandwidth, and narrow pulse [3], terahertz waves have broad application prospects in frontier technical fields such as optical communications systems [4], speed sensors [5], environmental monitoring [6], optical interconnect [7], biomedicine [8], and national defense technology [9]. The frequency band of terahertz determines that the generation of terahertz waves is a key subject in its development and application. Two traditional methods for generating terahertz waves are photonics and electronics [10]. In general, the photoconductive method generates terahertz waves with a higher intensity, while the optical rectification method provides a wider bandwidth. However, the optical rectification method can also obtain higher intensity in some cases, such as accelerator and germanium photoconductive antennas [11–13]. In other words, different terahertz sources also have different characteristics. Terahertz quantum cascade lasers have the advantages of considerable power, small size, compact structure, and adjustable frequency points [14]. The optically pumped far-infrared laser has higher power and a wider frequency band, but it also has the disadvantages of low

operating temperature, low efficiency, and large volume, which hinder its popularization and application [15]. In addition, the nonlinear difference frequency generation method has attracted wide attention because of its merits such as high power, low cost, and normal temperature operation, and the rapid development and in-depth exploration of photonic crystal provide more and better solutions for this method [16].

Therefore, Dr. Kitada's laboratory [17] has reported the development of a real-temperature cascade laser that emits a two-wavelength laser in the mid-infrared region and generates terahertz light by producing a different frequency in the resonator. The structure of this laser includes two resonators located in the high reflection region, which create terahertz waves through the frequency difference between them. However, this laser type has issues such as a high threshold current, heat generation, and low power conversion efficiency, which reduces device life and stability. Therefore, this study aims to address these problems by introducing a photonic crystal structure. By utilizing doped semiconductors in the photonic crystal, the absorption of terahertz waves is increased, and the second-order nonlinear optical effect is generated. Then, the improvements in the efficiency of terahertz generation and greater output were verified at the same time.

Photonic crystals play an essential role in the study of terahertz bands with the advantages of losslessness, low dispersion, and transparency [18]. As a new physical concept, the first photonic crystal fiber (PCF) was manufactured [19], and then a variety of new PCFs continued to emerge [20]. For example, an eight-channel C-band demux based on multicore photonic crystal fiber [21] and a 1×16 power splitter based on the structure of variable multicore photonic crystal fiber [22].

The first photonic bandgap PCF with a periodic structure in the cross-section was successfully developed, and the optical transmission was quickly proved to be guided based on the internal total emission refractive index. The invention and preparation of the band gap fiber for transmitting light in the air have been realized the optical transmission with ultra-low loss, ultra-low nonlinearity, and ultra-low dispersion [23]. Then, researchers created the highly birefringent PCF made of lead-bismuth-gallium silicate glass with anomalous dispersion characteristics, which enabled the supercontinuum spectrum to be obtained from the near-infrared to the mid-infrared (700–2500 nm) [24]. The rapid development of PCF theory and performance has driven their practical application [25]. Additionally, the decagonal PCF without complex cladding demonstrated high birefringence, low loss, and dispersion shift [26]. Meanwhile, a dual-wavelength laser in the mid-infrared region that works at room temperature was studied [27], which can obtain a terahertz optical quantum cascade laser through the difference frequency generated in the cavity.

Conventional surface-emitting lasers usually have multiple transverse and longitudinal modes, which limits the output efficiency of the hole-coupled output cavity to 50% in the terahertz band. A lot of research is focused on improving the coupling output efficiency and achieving wide-spectrum tunable output to meet the needs of high-density wavelength division multiplexing and dual-wavelength measurement. In this study, a new method of improving the optical confinement of the excitation light for THz and generating THz light was proposed by introducing a square-lattice photonic crystal structure into a vertical cavity surface emitting laser. The finite-difference time-domain method [28] was used to analyze the control effect of the photonic crystal structure on the transverse mode of the vertical cavity surface emitting laser and the release effect of light confinement of PN junction [29]. Finally, the simulation calculations were performed to enhance the optical confinement and increase the efficiency and output power of terahertz waves.

2. Theoretical and Computational Analysis

2.1. The Basic Structure of the Square-Lattice PhC-VCSEL

The photonic crystal vertical cavity surface emitting laser (PhC-VCSEL) with the square-lattice photonic crystal structure that consists of various layers stacked from top to bottom, including a p-type distributed Bragg reflector (DBR), an oxide layer, multiple quantum well (MQW), n-type DBR, GaAs cavity, undoped DBR and bottom contact [30].

The schematic diagram of a three-dimensional (3D) PhC-VCSEL is shown in Figure 1, and the laser is emitted from the surface of the photonic crystal structure, which contains a periodic air hole square lattice. The structure's refractive index difference is determined by its period and duty cycle, and the influence of the aperture and period of the photonic crystal defect on the visible light intensity must be considered. Using a 0.4 μm aperture and an 85 nm depth, with a duty ratio of 0.2 and a period of 1 μm, a single defect structure of the square photonic crystal can be achieved, as shown in Figure 1, where the polarization direction of the light is parallel to the X-axis.

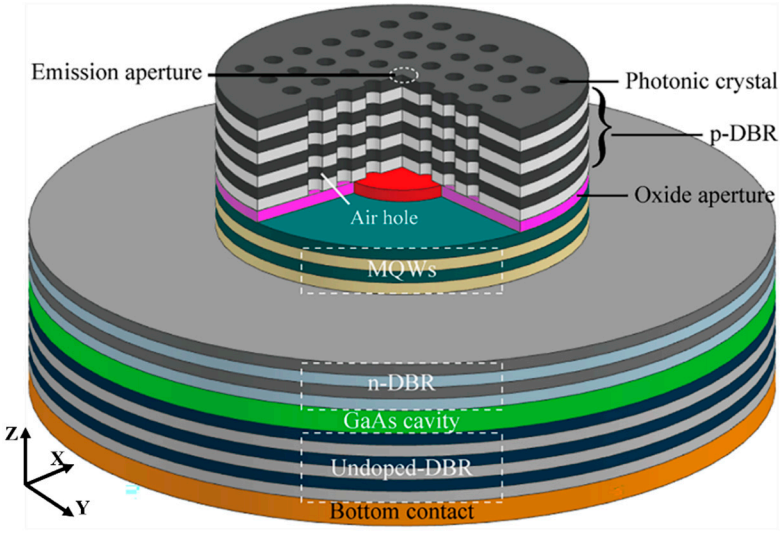

Figure 1. Schematic diagram of three-dimensional PhC-VCSEL.

Regarding the oxide layer, it is composed of AlAs and Al_2O_3, represented by red and pink materials, respectively. Specifically, the material composition of the other parts of the structure is listed in Table 1.

Table 1. Photonic crystal vertical resonator surface-emitting laser thickness.

Layer	Thickness (nm)	Material	Number of Plies
p-DBR	8/17	AlGaAs/GaAs	28 pairs
Oxide layer	30	$AlAs/Al_2O_3$	-
MQW cavity	16.8/3.6	GaAs/InGaAs	3 pairs
	16/4.4	GaAs/InGaAs	3 pairs
n-DBR	8/17	GaAs/AlGaAs	12.5 pairs
GaAs cavity	3/2λ	GaAs	-
Undoped-DBR	8/17	AlGaAs/GaAs	34 pairs
Bottom contact	-	GaAs (113) B substrate	-

In the case of a short cavity length, the light propagates perpendicular to the substrate with almost no unidirectional gain, which requires the light to reciprocate multiple times in the cavity to control the direction of the photons. In order to improve the photoelectric conversion efficiency, it is not only necessary to match the resonant wavelength of the resonant cavity, the maximum gain wavelength of the active area, and the reflection wavelength of the resonator mirror but also the lattice constant of the mirror material and the active area must be matched. In the vertical light distribution of the PhC-VCSEL, the maximum of the standing wave light intensity distribution appears at the quantum well position in the active region. So, the maximum optical gain can be obtained by rationally optimizing the position and number of quantum wells [31]. In addition, the single-defect structure of the photonic crystal can introduce mode loss into the transverse mode of the device, and the different positions of the transverse modes of different orders will

also make the different losses introduced by the VCSEL [32]. The high-order transverse modes will be suppressed due to the introduction of larger transverse losses, while its fundamental transverse modes are prone to lasing by introducing smaller losses. Therefore, the introduction of photonic crystals can effectively control the VCSEL to work in the fundamental transverse mode. Accurately, a square lattice photonic crystal structure was innovatively introduced into the vertical cavity surface emitting laser surface to improve the lateral-direction confinement of lasing light in near infrared in the above model.

2.2. Design of the Square Lattice Photonic Crystal Structure

The characteristics of photonic crystals make it possible to control the light propagation direction and realize light confinement in the vertical cavity surface of the laser [33]. Further, it can generate greater light intensity in regions with nonlinear optical characteristics, and it can be expected that the difference frequency can generate terahertz waves more effectively. To analyze the mechanism of the square photonic crystal structure, the periodically arranged hexagonal and quadrangular two-dimensional photonic crystal structures were designed, and the two types of photonic band gaps were investigated by the plane expansion method. In Figure 2, the profile, TE mode, and TM mode photonic band gap of the hexagonal lattice photonic crystal are represented by (a_1), (a_2), and (a_3), respectively. Likewise, the profile, TE mode, and TM mode photonic band gap of the square lattice photonic crystal are represented by (b_1), (b_2), and (b_3), respectively. The structures in Figure 2 are square photonic crystals and hexagonal photonic crystals with a size of 7×7, and their defects are located in the middle part, that is, point defects. The photonic bandgap characteristics of a photonic crystal rely on several parameters, such as the refractive index of the cylinder $n_2 = 1$, the lattice constant $a = 1$, and the radius of the cylinder $r = 0.2a$. Most importantly, the refractive index of the background medium n_1 was set to 3.52 to calculate the two-dimensional photonic crystal band gap of periodic cylindrical pores in a GaAs semiconductor thin film.

The photonic band gap of the photonic crystal structure is indicated by the blue bar. Obviously, different photonic crystal structures with the fixed filling factor correspond to different energy band structures. For the hexagonal type, the band gap of the photonic in TE mode is 0.346–0.352 a/λ, but the band gap of the photonic band gap in TM mode is 0.203–0.212 a/λ. However, the photonic bandgap of the square lattice photonic crystal can be obtained in a broader range. In the TE mode, the photonic bandgap is 0.436–0.528 a/λ, and in the TM mode, the photonic bandgap is 0.216–3.3 and 0.406–0.486 a/λ. As shown in Figure 2, the square photonic crystal can have a wider band gap, and it is easier to produce a complete forbidden band. According to the needs of the actual device, set the lattice constant of the photonic crystal, $r/a = 0.2$, so that the complete band gap can be fully utilized. As a result, a square lattice crystal with the filling factor of $r/a = 0.2$ is selected in the subsequent numerical calculations.

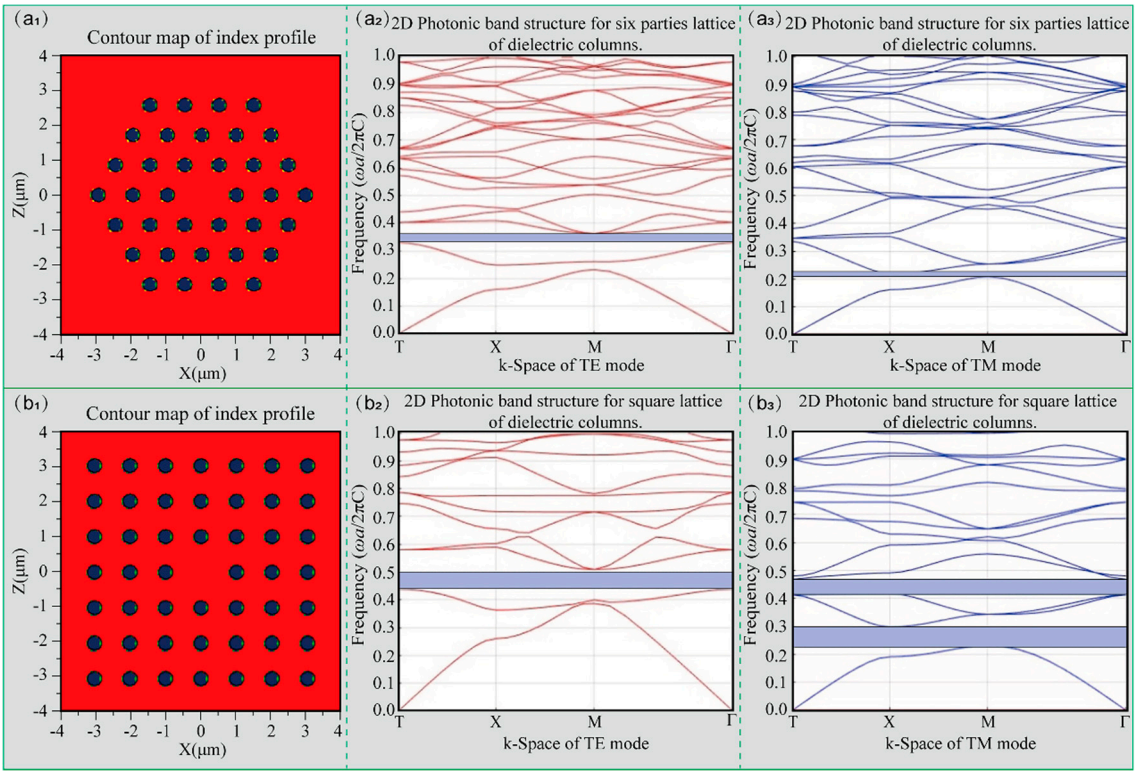

Figure 2. The calculated result of the photonic band gap in TE and TM mode. (**a1**) hexagonal photonic crystal structure, (**a2**) the calculated result of the hexagonal photonic band gap in TE mode, (**a3**) the calculated result of the hexagonal photonic band gap in TM mode, (**b1**) square photonic crystal structure, (**b2**) the calculated result of the square photonic band gap in TE mode, (**b3**) the calculated result of the square photonic band gap in TM mode.

3. Dielectric Constant Analysis of GaAs and Al*x*Ga1-*x*As

The dielectric constants of GaAs and $Al_xGa_{1-x}As$ are important parameters for designing and analyzing the terahertz band devices, and free carrier absorption plays a significant role in the terahertz optical properties of $Al_xGa_{1-x}As$ film materials [34]. The free carrier optical properties of GaAs and the dielectric constant response function of thin film samples can be reasonably described using the Drude model [35] and the Lorenz-Drude model [36]. The optical properties of p-type $Al_xGa_{1-x}As$ epitaxial film with beryllium and carbon doping concentrations of 10^{18}–10^{19} cm^{-3} have been investigated by far-infrared reflectance spectroscopy in the frequency range of 1.5–15 THz [37]. Figure 3 shows the optical layout of GaAs and $Al_xGa_{1-x}As$, and the three-layer air/film/substrate model was used to calculate the dielectric constant and analyze the optical properties of the film. Here, the complex refractive index of air, thin film, and substrate are set to n, n_f, and n_s, respectively.

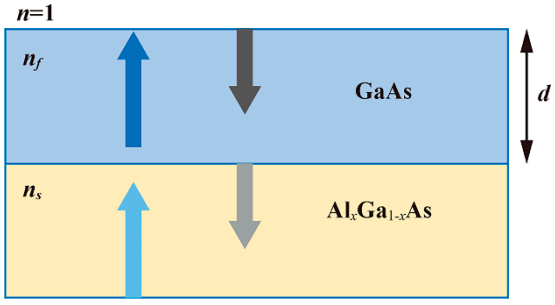

Figure 3. Optical layout of GaAs and $Al_xGa_{1-x}As$.

The GaAs in the layout above has an undoped concentration, and its dielectric function can be expressed by Lorentz resonance as

$$\varepsilon_{GaAs}(\omega) = \varepsilon_\infty \left(1 + \frac{\omega_{LO}^2 - \omega_{TO}^2}{\omega_{TO}^2 - \omega^2 - i\gamma\omega}\right) \tag{1}$$

where the ε_∞ is the metal dielectric constant at infinite frequency, ω is the terahertz frequency, γ is the damping factor, ω_{LO} and ω_{TO} are the vertical and horizontal optical phonon frequencies, respectively. Specifically, the real and imaginary parts of the dielectric function near the phonon frequency of GaAs optical are shown in Figure 4, and the values of each parameter are listed in Table 2.

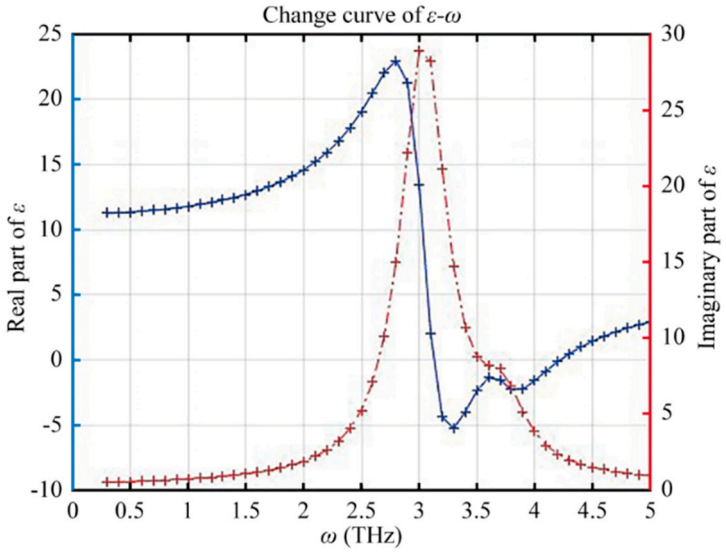

Figure 4. Optical properties of GaAs without carrier concentration (the bule line is real part, the red line is Imaginary part).

Table 2. Dielectric function parameter of GaAs [35].

ε_∞	ω_{LO}	ω_{TO}	γ
11	292.1 cm^{-1}	268.7 cm^{-1}	2.4 cm^{-1}
11	34.24 μm	37.22 μm	4166.67 μm

On the other hand, when there is a doping concentration in GaAs, its dielectric function [30] is expressed as

$$\varepsilon_{GaAs}(\omega) = \varepsilon_\infty - \frac{\varepsilon_\infty \omega_p^2}{\omega(\omega + i\gamma)} + \frac{\varepsilon_\infty(\omega_{LO}^2 - \omega_{TO}^2)}{\omega_{TO}^2 - \omega^2 - i\gamma\omega} \tag{2}$$

where ω_p is the plasma frequency. Further, the dielectric function of the $Al_xGa_{1-x}As$ film can be represented as follows

$$\varepsilon_{AlGaAs}(\omega) = \varepsilon_\infty - \frac{\varepsilon_\infty \omega_p^2}{\omega(\omega + i\gamma)} + \sum_{k=1}^{2} \frac{S_k(\omega_{LO}^2 - \omega_{TO}^2)}{\omega_{TO,k}^2 - \omega^2 - i\gamma\omega} \tag{3}$$

where $\omega_{TO,k}$ is the transverse optical TO phonon frequency, and S_k is the TO phonon intensity.

From previous research, the plasma frequency of $Al_xGa_{1-x}As$ is approximately linear with its effective mass [38]. This means that the plasma frequency will decrease with the increase of Al content in the case of the same carrier concentration, and Equation (3) indicates

that when the plasma frequency of a semiconductor exceeds the frequency of a terahertz wave, the dielectric constant for the terahertz wave becomes negative. Consequently, the terahertz surface plasma wave excited by $Al_xGa_{1-x}As$ can be propagated on the surface of the semiconductor. In addition, under the carrier concentration of 3.0×10^{18} cm^{-3} and 4.7×10^{18} cm^{-3}, the influence of Al content on the dielectric constant of $Al_xGa_{1-x}As$ was analyzed. It can be seen from Figure 5 that at the same frequency with the increase of Al content, the increase of the real part of the $Al_xGa_{1-x}As$ dielectric constant is accompanied by the decrease of the imaginary part. To broaden the range of terahertz wave frequencies, the p-type contact layer was heavily Be doped, the Al content was selected to be 0.01, and the carrier concentration was set to 3.0×10^{18} cm^{-3} in the follow-up simulation experiments.

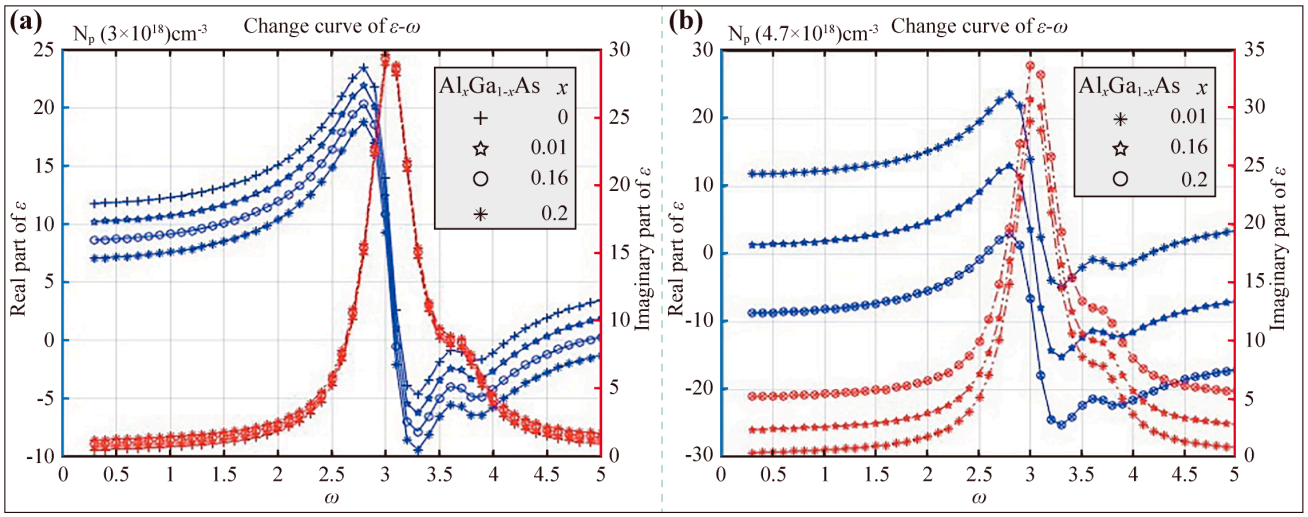

Figure 5. The influence of Al content on the dielectric constant of $Al_xGa_{1-x}As$. (**a**) The carrier concentration is 3.0×10^{18} cm^{-3}, (**b**) The carrier concentration is 4.7×10^{18} cm^{-3}.

4. Simulation Method and Calculation Model of VCSEL

As shown in Figure 6a, a 3D simulation model of the PhC-VCSEL was established, and the device size was set as 20 μm × 20 μm × 20 μm in the Fullwave software. The refractive index profiles without and with photonic crystal are exhibited in Figure 6b,c, respectively. In numerical calculation, the symmetric boundary conditions can be used to reduce the simulation area to 1/4 of the original size, and the mesh accuracy exceeds 1/10 of the wavelength, which can ensure the accuracy of the data. In addition, there are more layers in the Z direction of the device, and the light intensity distribution is concentrated, so the grid division needs to be more compact. The device is designed with a calculation area containing photonic crystal defect holes on the XY plane, a photonic crystal pore structure, and the thickness in the Z direction. Among them, the lattice constant of the holes arranged in a square lattice is 1 μm, and the radius r is 0.2 μm. In fact, the hole defect placed in the center is to form holes in the lateral molecules of the PN junction and prevent carriers from being injected into the active layer to form a flow. Therefore, the PN junction can excite the laser from the surface to the active layer. In this simulation device, a monitor was also set up to detect the electric field strength E^2 inside the entire device. Meanwhile, the center wavelength of the pulse wave source, pulse width, and polarization direction were set to 920 nm, 100 fs, and 90°, respectively. In addition, since the light intensity is mainly distributed in the multi-layer structure in the Z direction, the grid division of the calculation area needs to make the grid in the Z direction denser.

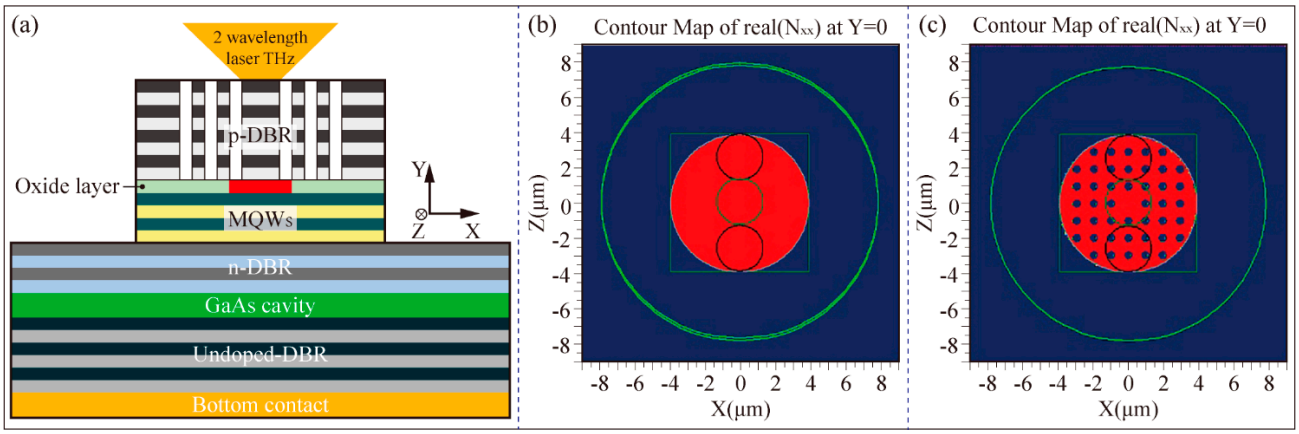

Figure 6. Simulation model and refractive index profile. (**a**) Schematic diagram of the device structure, (**b**) Cross-sectional view of the refractive index distribution without the photonic crystal structure, (**c**) Cross-sectional view of the refractive index distribution of the square photonic crystal structure.

5. The Influence of Photonic Crystal on the Optical Confinement of VCSEL

The resonant wavelength information on the device was detected by the monitor to analyze the influence of the photonic crystal on the optical confinement of the VCSEL in the terahertz band. In the absence of a photonic crystal structure, the resonance spectrum characteristics obtained by the Fourier transform of the time-varying curve of the electric field intensity are shown as the blue line in Figure 7. The blue line indicates that the peak of the electric field intensity lies between the wavelengths of 0.88 μm and 0.99 μm, which indicates that two wavelengths oscillate simultaneously in the vertical direction.

The red line in Figure 7 describes the resonant wavelength obtained by the monitor with a photonic crystal structure. The peak intensity appears between 0.83 μm and 1.05 μm, indicating that the two wavelengths not only oscillate simultaneously in the vertical direction but also have a larger difference frequency compared with devices without photonic crystal structure. The reason is that the unrestricted emission spectrum of photonic crystals has a side mode, the emission spot is distributed over the entire emission surface, and the oscillation mode is mainly limited by the oxidation holes. However, VCSELs are mainly limited by photonic crystal defects. In the PhC-VCSEL, two wavelengths are oscillated concurrently to generate a frequency difference through nonlinear optical effects, then a terahertz wave can be stimulated, and there is an adjustment range of 0.22 μm to control the difference frequency between the two wavelengths.

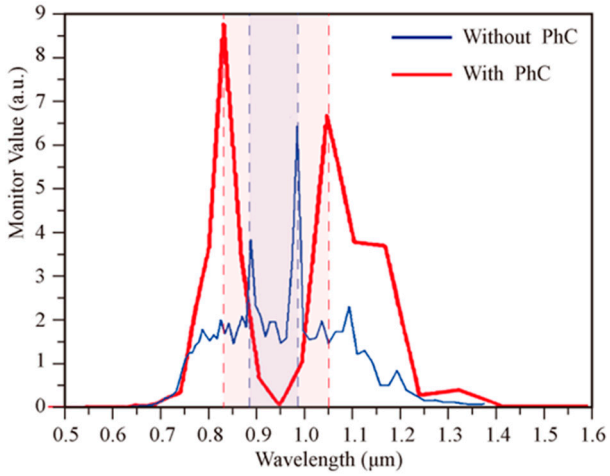

Figure 7. Resonance wavelengths of devices with or without photonic crystal structures. (red line) Without photonic crystal structure, (blue line) With photonic crystal structure.

In the terahertz band, the effects of photonic crystal and carrier concentration on the light confinement of the VCSEL are researched. Without the photonic crystal structure, the frequency f was set to 10 THz, and the wave source was placed in the active layer to determine the electromagnetic field distribution. First, the influence of the carrier concentration on the intensity of the outgoing photoelectric field in the terahertz region was analyzed. When the carrier concentration in GaAs and $Al_xGa_{1-x}As$ was set to 3.0×10^{18} cm^{-3}, and the dielectric constant ε_{AlGaAs} was set to $11 + i3.2 \times 10^{-3}$. The simulation results can be seen from Figure 8 that the penetration depth of light is about 4 mm, which has exceeded the size of the device, then the emitted terahertz light is weakened by the absorption of carriers. The absorption coefficient α is calculated as follows

$$\alpha = \frac{2\omega}{c}\kappa = \frac{2 \times 2 \times 3.14 \times 10 \times 10^{12} \times 0.0006}{3 \times 10^{8}} = 2.5 \times 10^{2}\ m^{-1} \quad (4)$$

where κ is the extinction coefficient of AlGaAs, and c is the velocity of light.

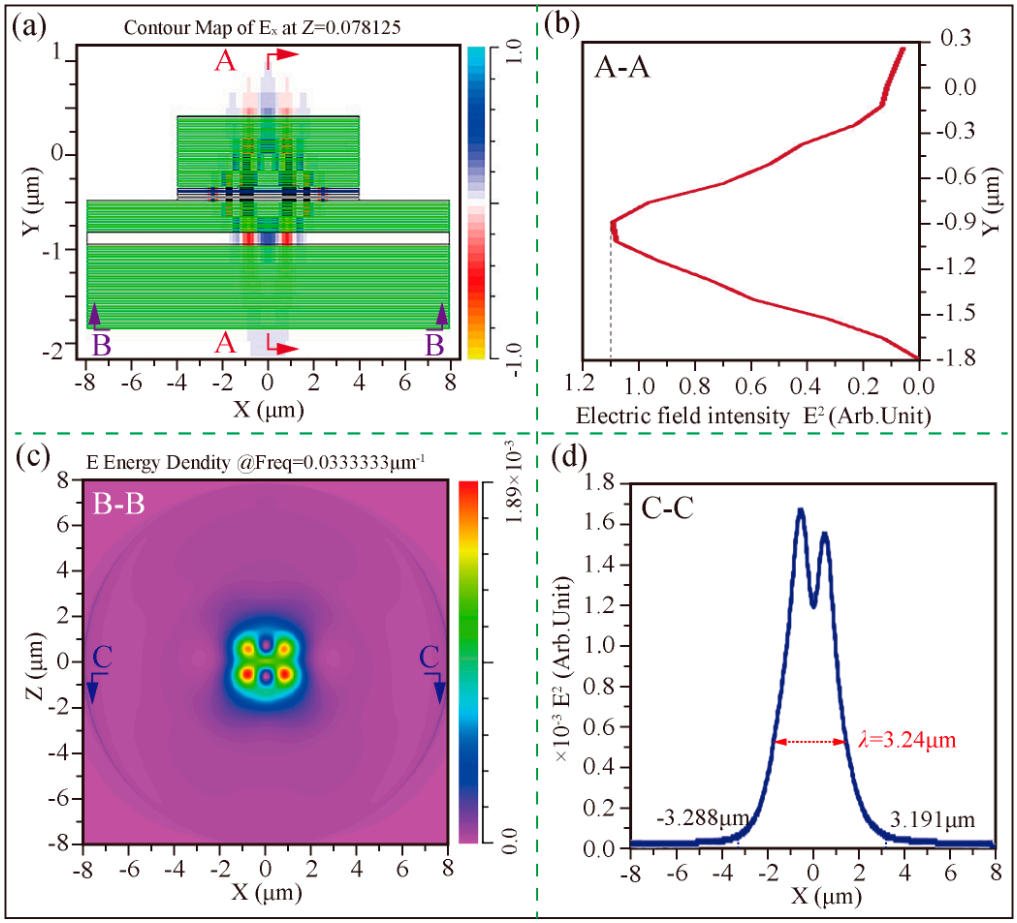

Figure 8. The E^2 distribution at the terahertz wave source without a photonic crystal device, and the carrier concentration in GaAs and $Al_xGa_{1-x}As$ is 0. (**a**) The XY cross-section, (**b**) E^2 in the A-A direction, (**c**) The XZ in the B-B cross-section, (**d**) E^2 in the C-C direction.

In addition, when the carrier concentration in GaAs and $Al_xGa_{1-x}As$ is 0, the electric field distribution at the terahertz wave source without and with photonic crystals is exhibited in Figures 8a and 9a, respectively. On the one hand, in the case of VCSELs without photonic crystals, the electric field intensity in the Y-axis direction is shown in Figure 8b, and its peak value is 1.1. It can be seen from the XZ cross-section of Figure 8c and the C-C direction of Figure 8d that the electric field intensity of the light emitted in the terahertz region is 1.69×10^{-3} and the half-width of the beam is 3.24 μm. On the other hand, in the

case of VCSELs with photonic crystals, the electric field intensity in the Y-axis direction is shown in Figure 9b and its peak value is 4.8, which is 4.36 times that of devices without photonic crystal. Similarly, the XZ cross-section of Figure 9c and the C-C direction of Figure 9d demonstrate that the electric field intensity of the light emitted in the terahertz region is 7.6×10^{-3} and the half-width of the beam is 1.06 µm. In other words, the peak electric field intensity of PhC-VCSEL is 6.33 times the peak electric field intensity of the device without the photonic crystal structure in the X-axis.

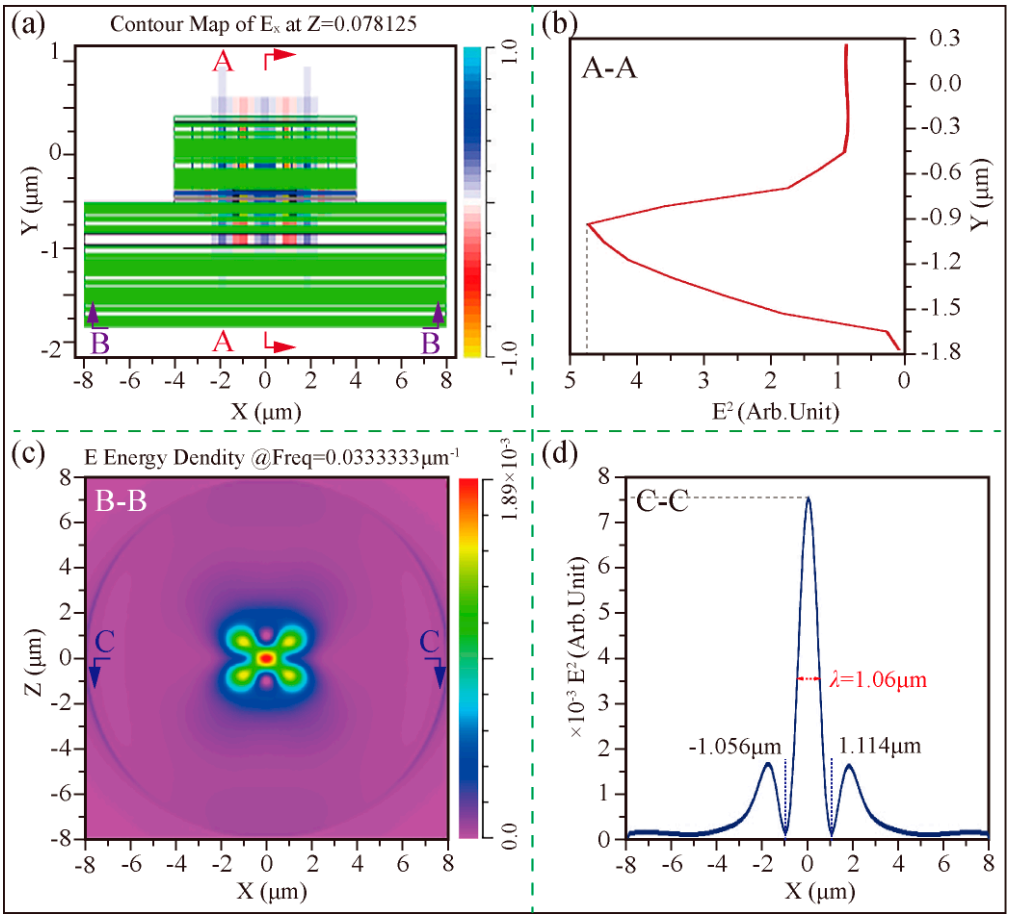

Figure 9. The E^2 distribution at the terahertz wave source with a photonic crystal device, and the carrier concentration in GaAs and $Al_xGa_{1-x}As$ is 0. (**a**) The XY cross-section, (**b**) E^2 in the A-A direction, (**c**) The XZ in the B-B cross-section, (**d**) E^2 in the C-C direction.

When the carrier concentration in $Al_xGa_{1-x}As$ was set to 3.0×10^{18} cm^{-3}, the frequency and the dielectric constant ε_{AlGaAs} were set to 10 THz and $11 + i3.2 \times 10^{-3}$, respectively. The optical confinement of VCSEL without and photonic crystal are shown in Figure 10. From the results without photonic crystals in Figure 10a,b, it can be seen that the penetration depth of light is about 4 mm, which has exceeded the size of the device, and the emitted terahertz light is weakened by the absorption of carriers. Similarly, the absorption coefficient is $\alpha = 2\omega\kappa/c = 2.5 \times 10^2$ m^{-1}. Furthermore, in the case of Figure 10c,d containing photonic crystal structures, the generated terahertz wave will not be emitted outside the device in this simulation.

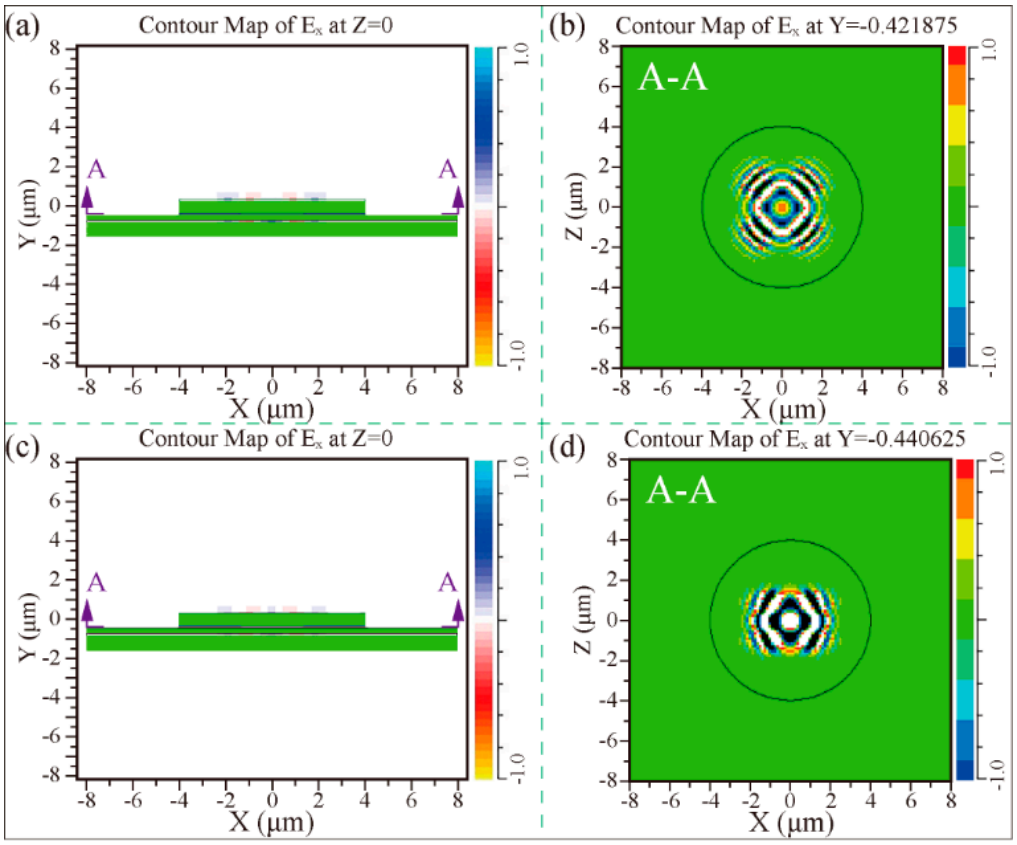

Figure 10. The E^2 distribution at the terahertz wave source with (down) and without (up) a photonic crystal device, the carrier concentration in $Al_xGa_{1-x}As$ was set to 3.0×10^{18} cm^{-3}. (**a**) E^2 distribution on the XY plane, (**b**) E^2 in the A-A distribution on the XZ plane, (**c**) E^2 distribution on the XY plane, and (**d**) E^2 in the A-A distribution on the XZ plane.

6. Conclusions

In this paper, a new method of introducing a square-lattice photonic crystal structure into the vertical cavity surface emitting laser was proposed to improve the optical confinement of the terahertz band. The mechanism is to use photonic crystal defects to form a light-limited resonant cavity. The cavity Q value can be maximized to form a single-mode cavity by changing the structure and arrangement of the photonic crystal. By using the total internal reflection of the air interface, the photon will be limited, and the output power will be increased in the vertical dimension of the defects. A three-dimensional model of a VCSEL with a photonic crystal structure was established, and the theoretical analysis was carried out to verify that this new structure can output and oscillate two terahertz laser beams in the vertical plane.

By calculating the energy band structure and optical band value of the photonic crystal, the filling factor of the square-lattice photonic crystal structure was optimized, and the optimal value of the optical band value was found to be 0.436~0.528 a/λ. Analysis of the optical properties of semiconductor materials in the terahertz band showed that the dielectric constant decreases with increasing free carrier concentration. The incident light wave in the terahertz band from 30 μm to 300 μm, the light in the photonic crystal vertical cavity surface emitting laser, will be confined in the DBR structure. In addition, the control effect of the photonic crystal structure on the transverse mode of the vertical cavity surface emitting laser and the release effect of the PN junction light confinement were investigated. The numerical calculation results illustrate that the difference in frequency intensity and optical field intensity of the vertical cavity surface emitting laser with the cubic photonic crystal structures can be increased by 2 and 6.33 times, respectively. In future research

work, the photonic crystal structure will be prepared by chemical vapor deposition and femtosecond laser two-photon technology to improve the performance of VCSEL.

Author Contributions: Conceptualization, Writing—original draft, Writing—review and editing, Methodology, Y.W.; Data Curation, Software, M.H.; Visualization, X.Z.; Methodology, Resources, P.W.; Supervision Writing—review and editing, S.S. All authors have read and agreed to the published version of the manuscript.

Funding: This research was funded by 111 project of China (Grant No. D21017); Belt and Road Innovative Talents Exchange Program, China (Grant No. DL2021025003L); National Natural Science Foundation of China (Grant No. 51775289); Major science and technology innovation project of Shandong Province (No. 2019JZZY010402); Key Research and Development Plan of Shandong Province, China (Grant No. 2019GGX104097); Natural Science Foundation of Shandong Province, China (Grant No. ZR2019BF050) and Qingdao Postdoctoral Applied Research Project.

Institutional Review Board Statement: Not applicable.

Informed Consent Statement: Not applicable.

Data Availability Statement: The data presented in this study are available on request from the corresponding authors.

Conflicts of Interest: The authors declare no conflict of interest.

References

1. Yakasai, I.K.; Abas, P.E.; Begum, F. Proposal of Highly Birefringent Porous Core Photonic Crystal Fibre for Polarisation Maintaining Terahertz Wave Guidance. In Proceedings of the IEEE 8th International Conference on Photonics (ICP), Kota Bharu, Malaysia, 12 May–30 June 2020. [CrossRef]
2. Němec, H.; Duvillaret, L.; Garet, F.; Kužel, P.; Xavier, P.; Richard, J.; Rauly, D. Thermally tunable filter for terahertz range based on a one-dimensional photonic crystal with a defect. *J. Appl. Phys.* **2004**, *96*, 4072–4075. [CrossRef]
3. Chassagneux, Y.; Colombelli, R.; Maineult, W.; Barbieri, S.; Beere, H.E.; Ritchie, D.A.; Khanna, S.P.; Linfield, E.H.; Davies, A.G. Electrically pumped photonic-crystal terahertz lasers controlled by boundary conditions. *Nature* **2009**, *457*, 174–178. [CrossRef] [PubMed]
4. Strzebonski, P.J.; North, W.; Jahan, N.; Choquette, K.D. Analysis of Coherence and Coupling in Vertical Cavity Surface Emitting Laser Arrays. *IEEE J. Quantum Electron.* **2022**, *58*, 1–8. [CrossRef]
5. Garnache, A.; Seghilani, M.; Sellahi, M.; Paquet, R.; Chomet, B.; Myara, M.; Blin, S.; LeGratiet, L.; Beaudoin, G.; Sagnes, I.; et al. Generation of new spatial and temporal coherent light states using III-V semiconductor laser technology: VORTEX, continuum, dual frequency for THz. *Phys. Chem. Appl. Nanostruct.* **2017**, *9734*, 471–474. [CrossRef]
6. Scalera, V.; Hudl, M.; Neeraj, K.; Perna, S.; D'Aquino, M.; Bonetti, S.; Serpico, C. Analysis in *k*-Space of Magnetization Dynamics Driven by Strong Terahertz Fields. *IEEE Trans. Magn.* **2020**, *57*, 1–5. [CrossRef]
7. Singh, G.; Kaur, G. Design and Implementation of Photonic Crystal Vertical Cavity Surface Emitting Laser. In Proceedings of the International Conference on Signal Processing and Communication (ICSC), Noida, India, 7–9 March 2019; pp. 32–36. [CrossRef]
8. Irfan, M.; Yim, J.-H.; Kim, C.; Lee, S.W.; Jho, Y.-D. Phase change in terahertz waves emitted from differently doped graphite: The role of carrier drift. *Appl. Phys. Lett.* **2013**, *103*, 201108. [CrossRef]
9. Liu, Y.; Yu, Z.; Liu, W.; Jia, Q.; Lu, Y. Terahertz Filters and Polarizers Using 2-D Subwavelength Hole Arrays. *IEEE Photon-J.* **2018**, *11*, 1–7. [CrossRef]
10. Kumar, S.; Williams, B.; Kohen, S.; Hu, Q.; Reno, J.L. High temperature continuous-wave operation of terahertz quantum cascade lasers. In Proceedings of the Conference on Lasers and Electro-Optics 1, San Francisco, CA, USA, 16–21 May 2004.
11. Tang, H.; Zhao, L.; Zhu, P.; Zou, X.; Qi, J.; Cheng, Y.; Qiu, J.; Hu, X.; Song, W.; Xiang, D.; et al. Stable and Scalable Multistage Terahertz-Driven Particle Accelerator. *Phys. Rev. Lett.* **2021**, *127*, 074801. [CrossRef]
12. Matlis, N.; Ahr, F.; Calendron, A.-L.; Cankaya, H.; Cirmi, G.; Eichner, T.; Fallahi, A.; Fakhari, M.; Hartin, A.; Hemmer, M.; et al. Acceleration of electrons in THz driven structures for AXSIS. *Nucl. Instrum. Methods Phys. Res. Sect. A Accel. Spectrometers Detect. Assoc. Equip.* **2018**, *909*, 27–32. [CrossRef]
13. Singh, A.; Pashkin, A.; Winnerl, S.; Welsch, M.; Beckh, C.; Sulzer, P.; Leitenstorfer, A.; Helm, M.; Schneider, H. Up to 70 THz bandwidth from an implanted Ge photoconductive antenna excited by a femtosecond Er:fibre laser. *Light. Sci. Appl.* **2020**, *9*, 1–7. [CrossRef]
14. Takigawa, S.; Noda, S. Mode analysis of two-dimensional photonic crystal terahertz lasers with gain/loss dispersion characteristics. *J. Opt. Soc. Am. B* **2010**, *27*, 2556–2567. [CrossRef]
15. Sultana, J.; Islam, S.; Faisal, M.; Islam, M.R.; Ng, B.W.-H.; Ebendorff-Heidepriem, H.; Abbott, D. Highly birefringent elliptical core photonic crystal fiber for terahertz application. *Opt. Commun.* **2018**, *407*, 92–96. [CrossRef]

16. Garai, S.K.; Mukhopadhyay, S. A method of optical implementation of frequency encoded different logic operations using second harmonic and difference frequency generation techniques in non-linear material. *Optik* **2010**, *121*, 715–721. [CrossRef]
17. Kitada, T.; Lu, X.; Minami, Y.; Kumagai, N.; Morita, K. Room-temperature two-color lasing by current injection into a GaAs/AlGaAs coupled multilayer cavity fabricated by wafer bonding. *Jpn. J. Appl. Phys.* **2018**, *57*, 04FH03. [CrossRef]
18. Suhara, T.; Avetisyan, Y.; Ito, H. Theoretical analysis of laterally emitting terahertz-wave generation by difference-frequency generation in channel waveguides. *IEEE J. Quantum Electron.* **2003**, *39*, 166–171. [CrossRef]
19. Russell, P.S.; Birks, T.A.; Knight, J.C.; Cregan, R.F.; Mangan, B.J.; De Sandro, J.-P. Silica/Air Photonic Crystal Fibres. *Jpn. J. Appl. Phys.* **1998**, *37*, 45. [CrossRef]
20. Cregan, R.F.; Mangan, B.J.; Knight, J.C.; Birks, T.A.; Russell, P.S.J.; Roberts, P.J.; Allan, D.C. Single-Mode Photonic Band Gap Guidance of Light in Air. *Science* **1999**, *285*, 1537–1539. [CrossRef]
21. Malka, D.; Katz, G. An Eight-Channel C-Band Demux Based on Multicore Photonic Crystal Fiber. *Nanomaterials* **2018**, *8*, 845. [CrossRef]
22. Malka, D.; Peled, A. Power splitting of 1 × 16 in multicore photonic crystal fibers. *Appl. Surf. Sci.* **2017**, *417*, 34–39. [CrossRef]
23. Chow, E.; Lin, S.Y.; Wendt, J.R.; Johnson, S.; Joannopoulos, J.D. Quantitative analysis of bending efficiency in photonic-crystal waveguide bends at λ = 1.55 μm wavelengths. *Opt. Lett.* **2001**, *26*, 286–288. [CrossRef]
24. Buczynski, R.; Bookey, H.; Pysz, D.; Stepien, R.; Kujawa, I.; McCarthy, J.; Waddie, A.; Kar, A.; Taghizadeh, M. Supercontinuum generation up to 2.5 μm in photonic crystal fiber made of lead-bismuth-galate glass. *Laser Phys. Lett.* **2010**, *7*, 666–672. [CrossRef]
25. Singer, A.M.; Hameed, M.F.O.; Heikal, A.M.; El-Mikati, H.A.; Obayya, S.S.A. Highly birefringent slotted core photonic crystal fiber for terahertz waveguiding. *Opt. Quantum Electron.* **2020**, *53*, 9. [CrossRef]
26. De, M.; Gangwar, R.K.; Singh, V.K. Designing of highly birefringence, dispersion shifted decagonal photonic crystal fiber with low confinement loss. *Photon- Nanostructures Fundam. Appl.* **2017**, *26*, 15–23. [CrossRef]
27. Kitada, T.; Tanaka, F.; Takahashi, T.; Morita, K.; Isu, T. GaAs/AlAs coupled multilayer cavity structures for terahertz emission devices. *Appl. Phys. Lett.* **2009**, *95*, 111106. [CrossRef]
28. Rzesnicki, T.; Piosczyk, B.; Kern, S.; Illy, S.; Jin, J.; Samartsev, A.; Schlaich, A.; Thumm, M. 2.2-MW Record Power of the 170-GHz European Preprototype Coaxial-Cavity Gyrotron for ITER. *IEEE Trans. Plasma Sci.* **2010**, *38*, 1141–1149. [CrossRef]
29. Czyszanowski, T.; Sarzała, R.P.; Dems, M.; Nakwaski, W.; Thienpont, H.; Panajotov, K. Optimal photonic-crystal parameters assuring single-mode operation of 1300 nm AlInGaAs vertical-cavity surface-emitting laser. *J. Appl. Phys.* **2009**, *105*, 093102. [CrossRef]
30. Liu, A.; Xing, M.; Qu, H.; Chen, W.; Zhou, W.; Zheng, W. Reduced divergence angle of photonic crystal vertical-cavity surface-emitting laser. *Appl. Phys. Lett.* **2009**, *94*, 191105. [CrossRef]
31. Xu, K.; Fang, M.; Huang, Z. Compact vertical-cavity surface-emitting laser based on all-dielectric metasurfaces. *Opt. Commun.* **2020**, *475*, 126257. [CrossRef]
32. Song, D.-S.; Kim, S.-H.; Park, H.-G.; Kim, C.-K.; Lee, Y.H. Single-mode photonic-crystal vertical cavity surface emitting laser. In Proceedings of the Conference on Lasers and Electro-Optics, Long Beach, CA, USA, 19–22 May 2002. [CrossRef]
33. Fernandes, H.C.C.; Medeiros, J.L.G.; Junior, I.M.A.; Brito, D.B. Photonic Crystal at Millimeter Waves Applications. *PIERS Online* **2007**, *3*, 689–694. [CrossRef]
34. Hu, Z.G.; Rinzan, M.B.M.; Matsik, S.G.; Perera, A.G.U.; Von Winckel, G.; Stintz, A.; Krishna, S. Optical characterizations of heavily doped p-type AlxGa1−xAs and GaAs epitaxial films at terahertz frequencies. *J. Appl. Phys.* **2005**, *97*, 093529. [CrossRef]
35. Vassant, S.; Pardo, F.; Bouchon, P.; Marquier, F.; Greffet, J.J.; Pelouard, J.L. Optical control of THz reflectivity with surface waves. *Proc. SPIE-Int. Soc. Opt. Eng.* **2011**, *8119*, 81190H. [CrossRef]
36. Yee, K. Numerical solution of initial boundary value problems involving Maxwell's equations in isotropic media. *IEEE Trans. Antennas Propag.* **1966**, *14*, 302–307. [CrossRef]
37. Lee, Y.-S. *Principles of Terahertz Science and Technology*; Springer: Berlin/Heidelberg, Germany, 2009. [CrossRef]
38. Herasimovich, A.; Shokhovets, S.; Goldhahn, R.; Gobsch, G. The dielectric function of a GaAs/AlGaAs single quantum well: Calculation and comparison with experiment. *Thin Solid Films* **2004**, *450*, 199–202. [CrossRef]